H_∞ optimization of multiple tuned mass dampers for multimodal vibration control

G. Raze[a,*], G. Kerschen[a]

[a] *Space Structures and Systems Laboratory, Aerospace and Mechanical Engineering Department, University of Liège Quartier Polytech 1 (B52/3), Allée de la Découverte 9, B-4000 Liège, Belgium*

Abstract

In this paper, a new computational method for the purpose of multimodal vibration mitigation using multiple tuned mass dampers is proposed. Classically, the minimization of the maximum amplitude is carried out using direct H_∞ optimization. However, as shall be shown in the paper, this approach is prone to being trapped in local minima, in view of the nonsmooth character of the problem at hand. This is why this paper presents an original alternative to this approach through norm-homotopy optimization. This approach, combined with an efficient technique to compute the structural response, is shown to outperform direct H_∞ optimization in terms of speed and performance. Essentially, the outcome of the algorithm leads to the concept of *all-equal-peak design* for which all the controlled peaks are equal in amplitude. This unique design is new with respect to the existing body of knowledge.

Keywords: multiple tuned mass damper, multimodal vibration absorber, equal-peak method, all-equal-peak design, Sherman-Morrison-Woodbury formula

1. Introduction

Tall, slender and light structures are more and more used in various engineering fields for performance, compliance with regulations and/or esthetic reasons. An inconvenient feature of these structures is their proneness to exhibit lightly-damped, high-amplitude resonances. Such resonances may shorten the lifetime of these structures and even render them dangerous for human use. A possible cure against this is to attach a tuned mass damper (TMD) to the structure in the attempt to mitigate its vibratory amplitude.

*Corresponding author

Email addresses: g.raze@uliege.be (G. Raze), g.kerschen@uliege.be (G. Kerschen)

The TMD was originally proposed by Frahm [1] as a spring-mass device for suppressing a specific resonance frequency. Ormondroyd and Den Hartog [2] added a damper to this device and tuned the resulting absorber based on fixed points of the compliance (i.e., the transfer function between a displacement of interest and the external forcing amplitude) of the controlled structure. The fixed points, independent on absorber damping, were chosen to be equal in amplitude. Brock [3] proposed a particular value of the absorber damping coefficient such that the two fixed points simultaneously be approximate maxima of the compliance. Those developments, gathered in Den Hartog's book [4], laid down the foundations of the *equal-peak design* because the controlled compliance exhibits two peaks of (approximately) equal amplitude, usually much lower than that of the uncontrolled structure. Since then, there has been a large number of tuning formulas varying with the loading conditions and objectives at hand. For instance, Warburton [5] who proposed an unified approach for the fixed-point method gave optimal parameters for several cases. Nishihara and Asami [6] found the exact analytical solution to the H_∞-optimization problem by minimizing the maximum value of the compliance under the assumption that the latter exhibits two peaks of equal amplitude (i.e., an exact equal-peak design).

TMDs are used in a wide range of civil and mechanical engineering applications. Reviews on the subject can be found in the works of Soto and Adeli [7] and Elias and Matsagar [8]. However, being *tuned* to a particular frequency, the TMD may feature a lack of robustness when the targeted resonance frequency is uncertain or varies with time. A solution to this issue can be to increase the mass of the absorber. As this is often a limiting factor, non-conventional TMDs can be used, such as proposed by De Angelis et al [9], wherein masses already present on the structure having structural or architectural functions are additionally used as tuned masses. Alternatively, an inerter can be added to TMDs in order to increase their inertance while increasing their actual mass to a lesser extent, see, e.g., De Domenico and Ricciardi [10]. A recent approach proposed by Dell'Elce et al [11] tunes the absorber parameters according to the maximum uncertainty on the host structure. Structural nonlinearities may also detune the absorber, but their effect can be countered effectively using a nonlinear tuned vibration absorber [12]. Alternatively, a number of small TMDs tuned over a frequency band centered around the resonance frequency of interest can be robust to variations in that frequency, but also more efficient than a single TMD in the sense that it yields a smaller minimum of maximum amplification. The beneficial effects of a TMD array were first discovered by

Snowdon [13] and Iwanami and Seto [14], but the true potential of multiple tuned mass dampers (MTMDs) was unlocked in the works of Igusa and Xu [15], Yamaguchi and Harpornchai [16] and Abe and Fujino [17], among others.

MTMD can also target multiple resonances by assigning one or several TMDs per mode to be controlled. Early works about multimodal vibration mitigation used bars [18] and beams [19–21] as host structures. Rana and Soong [22] applied this approach to spring-mass systems and, as their discussion reveals, this second use of MTMD received less attention than the first one. In those studies, the absorbers were tuned such that the controlled compliance displays two pairs of equal peaks in place of the first two resonances. Clark [23] demonstrated the MTMD efficiency in reducing the maximum acceleration experienced at the top of a building during an earthquake. Yau and Yang [24] robustly controlled two modes of cable-stayed bridges traveled by high-speed trains, by using one TMD array per mode to be controlled.

Closed-form expressions for the absorber parameters are usually available when the absorber is placed on undamped single-degree-of-freedom oscillators. They can also be used for multiple-degree-of-freedom structures provided that their resonance frequencies are widely spaced. Real-life structures always violate these assumptions to some extent. Krenk and Høgsberg [25] proposed to use quasi-static and quasi-dynamic background correction terms to account for non-resonant modes. Several numerical optimization techniques were used to tune TMD and MTMD parameters; examples include parameters space exploration [26, 27], gradient-based optimization [5, 28–35], metaheuristic optimization (such as particle swarm optimization [36, 37], genetic algorithms [38–40], harmony search [41–43], ant colony optimization [44, 45], simulated annealing [46] and coral reefs optimization [47]) and hybrid optimization algorithms, using both metaheuristic and gradient-based optimizations [48]. The aforementioned optimization procedures suffer from at least one of the following limitations. First, some of them neglect the effect of damping and/or other non-resonant structural modes in the structure. Second, metaheuristic optimization algorithms can be prohibitive in terms of computational cost when the number of variables to optimize becomes large. Finally, one or several absorber parameters are often assumed to be fixed, which may lead to a suboptimal design.

This paper proposes a novel MTMD tuning methodology for multimodal vibration mitigation of linear structures. The developed algorithm finds the resonance peaks of the compliance and

minimizes their amplitude simultaneously. It results in a so-called *all-equal-peak design*, i.e., all the peaks of the controlled resonances are equal in amplitude. The paper is organized as follows. In Section 2, the general principles of the tuning methodology approach and of the optimization algorithm are introduced. Section 3 details the numerical optimization procedure. Section 4 then illustrates the concept of all-equal-peak design with a simple spring-mass system and a simply supported plate featuring high modal density. Finally, the conclusions of the present study are drawn in Section 5.

2. A norm-homotopy approach for H_∞ optimization

In this paper, the structure without absorbers and with N_a attached absorbers is referred to as *host structure* and *controlled structure*, respectively. In the presence of harmonic forcing, the vibratory amplitude of a single-degree-of-freedom host structure is classically mitigated through the minimization of the H_∞ norm of a given transfer function, i.e., its maximum amplitude, resulting in the equal-peak design for which there exist well-established analytical tuning rules, e.g., [6]. However, multiple-degree-of-freedom host structures have more complicated transfer functions, which rules out the possibility of tuning the absorbers analytically. Resorting to numerical optimization for minimizing the H_∞ norm is then necessary.

When considering multiple resonances, one inherent difficulty with the H_∞ norm is that it considers only the resonance peak exhibiting the largest amplitude, i.e., it disregards the other controlled peaks. Their amplitude is thus minimized later in the optimization process when they themselves feature the largest amplitude. This typically results in a nonsmooth cost function which may lead to a premature termination of the algorithm. The alternative strategy proposed in this paper relies on a norm-homotopy optimization during which problems of increasing complexity are solved sequentially using the previously-obtained parameters as an initial guess for the next problem. Specifically, the p-norm of the vector containing the controlled peak amplitudes, i.e., $\|\mathbf{x}\|_p = (\sum_{i=1}^{n} |x_i|^p)^{1/p}$, is minimized, and p is sequentially increased so as to approach the H_∞ norm, as schematically presented in Fig. 1. A low value of p puts more weight on the resonance peaks with lower amplitudes and makes the optimization problem less stiff, whereas the subsequent increase in p ensures that resonances with large amplitudes are penalized enough. This approach does not theoretically guarantee to find the global minimum of the H_∞ norm, but it enables a significant improvement of the local optimum found by a direct H_∞ optimization, as will be shown

in the examples.

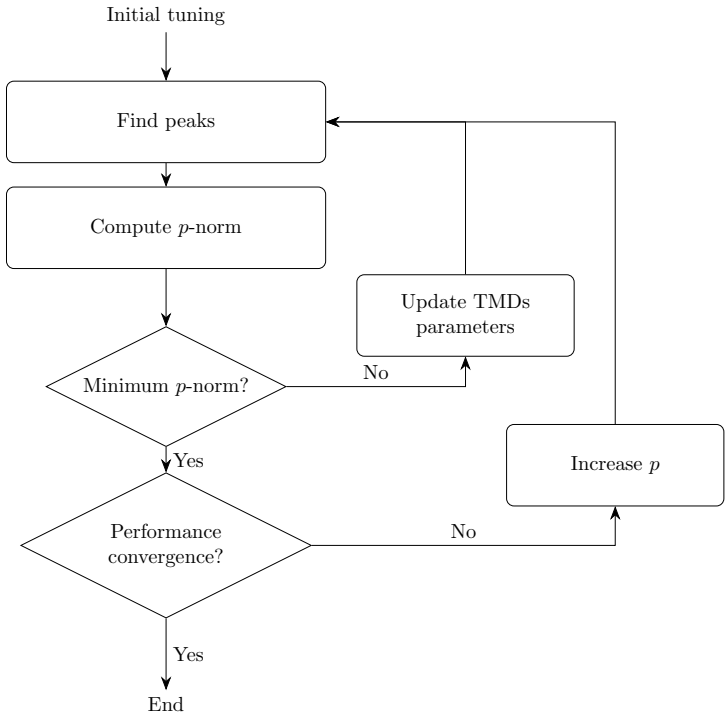

Figure 1: Conceptual flowchart of the proposed norm-homotopy optimization algorithm.

A typical output of the norm-homotopy optimization is shown in Fig. 2 for the mitigation of the resonances of a two-degree-of-freedom system (studied more in depth in Section 4.1). Clearly, the algorithm is able to enforce the same amplitude for the four resonances. Existing algorithms in the literature, see, e.g., [21], can also enforce equal peaks for each resonance, but the amplitudes associated with each pair of peaks are not equal, and the transfer function thus exhibits a higher H_∞ norm. This all-equal-peak design appears as a generalization to multiple modes of the equal-peak design, and can only be achieved through numerical optimization, given the complexity of the problem at hand.

3. The proposed optimization algorithm

The objective is to optimize the parameters of the different absorbers (mass, damping and stiffness) gathered in a vector $\boldsymbol{\xi}$. A tuning based on the well-established single-degree-of-freedom formulas from the literature provides an initial guess $\boldsymbol{\xi}_0$. The resulting performance is usually not satisfactory, and the parameters have to be optimized. As discussed in Section 2 and illustrated in

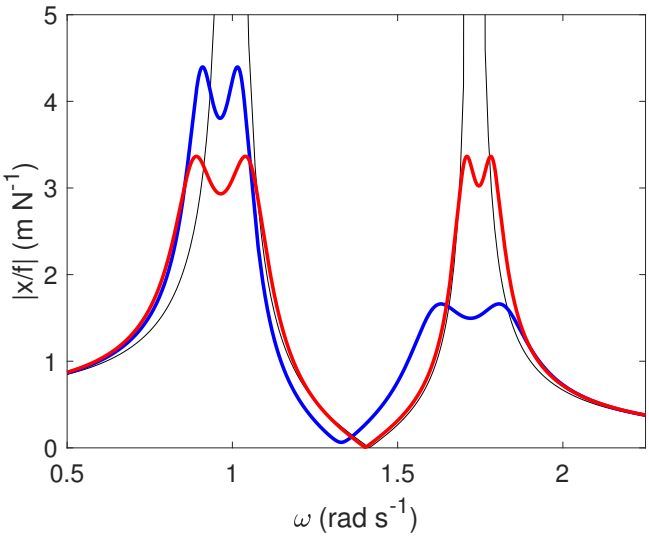

Figure 2: MTMD applied to a two-degree-of-freedom system: uncontrolled structure (—), solution from [21] (—) and norm-homotopy solution (—).

Figure 1, the proposed algorithm is based on successive optimizations of the p-norm of the vector containing the resonance peaks amplitude to avoid a nonsmooth objective function. The algorithm relies extensively on evaluations of the compliance, which may become computationally expensive for structures with a large number of degrees of freedom. To cope with this issue the dynamics of the controlled structure are formulated using the Sherman-Morrison-Woodbury formula [49].

3.1. Initial tuning

A MTMD with one TMD per targeted mode is considered herein, and we assume that the n^{th} absorber targets the n^{th} resonant mode of the host structure. It may be shown (see Appendix A or [5]) that, if one neglects non-resonant modes, the structure acts from the absorber point of view as an equivalent one-degree-of-freedom mechanical oscillator with the following modal mass, damping and stiffness:

$$m_n = \frac{1}{\phi_{a,n}^2}, \qquad c_n = 2\omega_n m_n \zeta_n, \qquad k_n = \omega_n^2 m_n \tag{1}$$

where $\phi_{a,n}$ is the n^{th} mass-normalized mode shape of the host structure at the location where the absorber is attached, ω_n is the resonance frequency, and ζ_n is the modal damping ratio. Classical formulas from the literature can then be used for absorber tuning ([4–6] or even [50] if damping in the host structure is taken into account). In this paper, the formulas from Nishihara and Asami [6]

are used. Since they are exact in the undamped single-degree-of-freedom case, they are expected to be a reasonably accurate initial guess for a multiple-degree-of-freedom case. From Eq. (1) the modal mass ratio for an absorber of mass $m_{a,n}$ is defined as

$$\mu_{a,n} = \frac{m_{a,n}}{m_n}, \tag{2}$$

and the absorber stiffness and damping are computed as

$$k_{a,n} = \frac{8}{(1+\mu_{a,n})^2} \frac{16 + 23\mu_{a,n} + 9\mu_{a,n}^2 + 2(2+\mu_{a,n})\sqrt{4+3\mu_{a,n}}}{3(64 + 80\mu_{a,n} + 27\mu_{a,n}^2)} \omega_n^2 m_{a,n} \tag{3}$$

$$c_{a,n} = \frac{1}{2}\sqrt{\frac{8 + 9\mu_{a,n} - 4\sqrt{4+3\mu_{a,n}}}{1+\mu_{a,n}}}\sqrt{k_{a,n} m_{a,n}}, \tag{4}$$

respectively. With these formulas, the maxima of the compliance are expected to be near the two resonance frequencies ω_{n1} and ω_{n2} defined by

$$\omega_{n1,n2} = \frac{1}{1+\mu_{a,n}} \left(1 \pm \sqrt{\frac{\mu_{a,n}}{2+\mu_{a,n}}}\right) \omega_n. \tag{5}$$

If maximum efficiency is sought, the modal mass ratio should be maximized [6], which, according to Eq. (2), is equivalent to minimizing the modal mass m_n. Going back to Eq. (1), the modal mass is minimized if the absorber is placed at a maximum of modal amplitude of the n^{th} mode in the host structure. This result is by no means new; further considerations are given in Petit et al [51] when either this location is not acceptable for attaching an absorber, or when the activity of the neighboring modes is too prominent.

This procedure can be repeated for each absorber to yield an initial design for the attached MTMD. For illustration, a damped single-degree-of-freedom host structure controlled by a single TMD, is studied through Section 3. Its purpose is to demonstrate the working principles of the algorithm with a simple example. The parameters of the host structure are $m_0 = 1$ kg, $k_0 = 1$ N m^{-1} and $c_0 = 0.02$ kg s^{-1}, giving rise to 1% modal damping. The mass ratio between the absorber and the host structure is 5%. Fig. 3 shows that the peaks of the compliance are unbalanced. Neither the fixed-point tuning [4] nor the exact H_∞ tuning [6] yield balanced peaks because of the presence of damping in the host. Unlike the H_2 norm optimization case, there is no closed-form solution to this problem [50]. The initial tuning is thus to be improved.

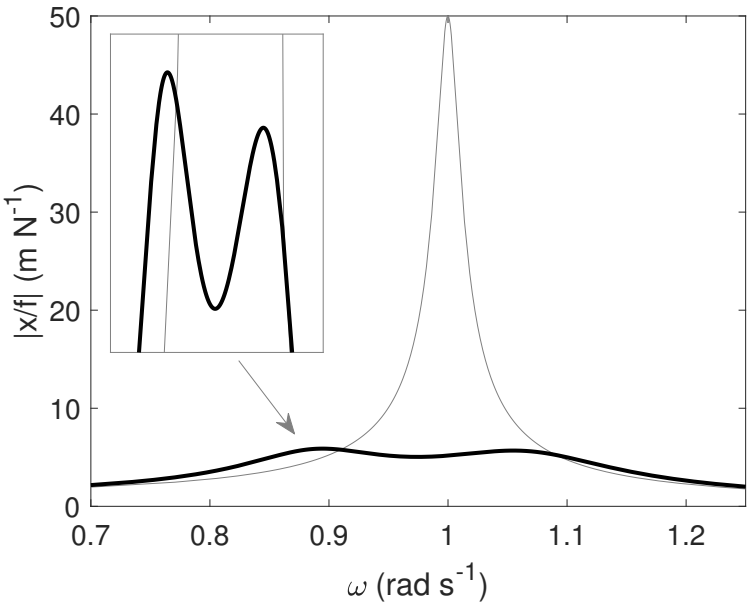

Figure 3: Compliance of the damped single-degree-of-freedom system: uncontrolled (—) and controlled (—) structure.

3.2. Dynamics of a structure with multiple tuned mass dampers

3.2.1. Dynamics of the uncontrolled structure

The dynamics of the discretized host structure is governed by the set of N coupled linear second-order ordinary differential equations (ODEs)

$$\mathbf{M}_0\ddot{\mathbf{x}} + \mathbf{C}_0\dot{\mathbf{x}} + \mathbf{K}_0\mathbf{x} = \mathbf{f}, \tag{6}$$

where $\mathbf{M}_0$, $\mathbf{C}_0$ and $\mathbf{K}_0$ are the structural mass, damping and stiffness matrices, respectively, $\mathbf{x}$ is the vector of generalized coordinates and $\mathbf{f}$ is the vector of conjugated generalized forces. Subscript 0 refers to the host structure, and an upper dot ($\dot{}$) denotes time derivation. Assuming harmonic forcing at angular frequency ω, the Fourier transform of Eq. (6) is given by

$$\left(-\omega^2\mathbf{M}_0 + j\omega\mathbf{C}_0 + \mathbf{K}_0\right)\mathbf{X}(\omega) = \mathbf{H}_0(\omega)\mathbf{X}(\omega) = \mathbf{F}(\omega). \tag{7}$$

j is the unit imaginary number (i.e., $j^2 = -1$), $\mathbf{X}$ and $\mathbf{F}$ are the Fourier transforms of $\mathbf{x}$ and $\mathbf{f}$, respectively, and $\mathbf{H}_0$ is the dynamic stiffness matrix. Because the host structure is in general lightly damped, the assumption of proportional damping is made. Using a modal expansion of the displacement and projecting the equations of motion onto the modal basis, the following inverse relation can be derived [52]:

$$\mathbf{X}(\omega) = \mathbf{H}_0^{-1}(\omega)\mathbf{F} = \mathbf{\Phi}_0\left(-\omega^2\mathbf{I} + 2j\omega\mathbf{Z}_0\mathbf{\Omega}_0 + \mathbf{\Omega}_0^2\right)^{-1}\mathbf{\Phi}_0^T\mathbf{F}(\omega), \tag{8}$$

where $\mathbf{\Phi}_0$ is the matrix of the mass-normalized mode shapes, $\mathbf{I}$ is the identity matrix, $\mathbf{\Omega}_0$ is a diagonal matrix containing the undamped resonance frequencies of the structure and $\mathbf{Z}_0$ is a diagonal matrix containing the associated modal damping coefficients. The superscript T denotes matrix transposition. In the remainder of this article, the modal expansion given by Eq. (8) is assumed to be known, so that $\mathbf{H}_0^{-1}$ is known as well.

3.2.2. Dynamics of the controlled structure

The dynamic equations of the controlled structure with N_a absorbers are given by the set of $N + N_a$ ODEs

$$\begin{gathered}\begin{bmatrix} \mathbf{M}_0 & \mathbf{0} \\ \mathbf{0} & \mathbf{M}_a \end{bmatrix} \begin{bmatrix} \ddot{\mathbf{x}} \\ \ddot{\mathbf{x}}_a \end{bmatrix} + \begin{bmatrix} \mathbf{C}_0 + \mathbf{B}\mathbf{C}_a\mathbf{B}^T & -\mathbf{B}\mathbf{C}_a \\ -\mathbf{C}_a\mathbf{B}^T & \mathbf{C}_a \end{bmatrix} \begin{bmatrix} \dot{\mathbf{x}} \\ \dot{\mathbf{x}}_a \end{bmatrix} + \\ \begin{bmatrix} \mathbf{K}_0 + \mathbf{B}\mathbf{K}_a\mathbf{B}^T & -\mathbf{B}\mathbf{K}_a \\ -\mathbf{K}_a\mathbf{B}^T & \mathbf{K}_a \end{bmatrix} \begin{bmatrix} \mathbf{x} \\ \mathbf{x}_a \end{bmatrix} = \begin{bmatrix} \mathbf{f} \\ \mathbf{0} \end{bmatrix},\end{gathered} \tag{9}$$

where $\mathbf{x}_a$ is the vector of generalized coordinates associated with the absorbers, $\mathbf{B}$ is a localization matrix collecting every localization vector $\mathbf{b}_n$ associated with the n^{th} absorber

$$\mathbf{B} = [\mathbf{b}_1 \ , \ \cdots \ , \ \mathbf{b}_{N_a}] \, , \tag{10}$$

and $\mathbf{M}_a$, $\mathbf{C}_a$ and $\mathbf{K}_a$ are diagonal matrices containing TMD parameters

$$\mathbf{M}_a = \begin{bmatrix} m_{a,1} & & \\ & \ddots & \\ & & m_{a,N_a} \end{bmatrix}, \qquad \mathbf{C}_a = \begin{bmatrix} c_{a,1} & & \\ & \ddots & \\ & & c_{a,N_a} \end{bmatrix}, \qquad \mathbf{K}_a = \begin{bmatrix} k_{a,1} & & \\ & \ddots & \\ & & k_{a,N_a} \end{bmatrix}. \tag{11}$$

Expressing the equations of motion in the frequency domain, it is possible to derive the compliance matrix in a manner similar to Eqs. (7)–(8). The burden associated with computing the compliance may however be alleviated by the Sherman-Morrison-Woodbury (SMW) formula [49]

$$(\mathbf{A} + \mathbf{U}\mathbf{Q}\mathbf{V})^{-1} = \mathbf{A}^{-1} - \mathbf{A}^{-1}\mathbf{U}\left(\mathbf{Q}^{-1} + \mathbf{V}\mathbf{A}^{-1}\mathbf{U}\right)^{-1}\mathbf{V}\mathbf{A}^{-1}. \tag{12}$$

for invertible matrices $\mathbf{A}$ and $\mathbf{Q}$. The principles of this alleviation were proposed in previous works. Ozer and Royston [53] used the Sherman-Morrison formula [54] as a simplifying numerical tool to tune the parameters of one absorber. Štepánekand Máca [35] recently used that formula recursively to adapt it to multiple absorbers. Another generalization to multiple lumped elements based on

the SMW formula was also proposed by Cha [55], but no attempt was made to use the formula to tune the absorbers.

The Fourier transform of the second line of Eq. (9) yields

$$\mathbf{X}_a(\omega) = \left(-\omega^2\mathbf{M}_a + j\omega\mathbf{C}_a + \mathbf{K}_a\right)^{-1}\left(j\omega\mathbf{C}_a + \mathbf{K}_a\right)\mathbf{B}^T\mathbf{X}(\omega). \tag{13}$$

Inserting this relation back into the Fourier transform of the first line of Eq. (9), one gets

$$\left(\mathbf{H}_0(\omega) + \mathbf{B}\left\{j\omega\mathbf{C}_a + \mathbf{K}_a - \left(j\omega\mathbf{C}_a + \mathbf{K}_a\right)\left(-\omega^2\mathbf{M}_a + j\omega\mathbf{C}_a + \mathbf{K}_a\right)^{-1}\left(j\omega\mathbf{C}_a + \mathbf{K}_a\right)\right\}\mathbf{B}^T\right)\mathbf{X}(\omega) = \mathbf{F}(\omega). \tag{14}$$

Carrying out simplifications on the diagonal matrices related to the absorbers, the dynamic stiffness matrix of the controlled structure $\mathbf{H}_c$ can be expressed as

$$\mathbf{H}_c(\omega) = \mathbf{H}_0(\omega) + \mathbf{B}\mathbf{H}_A(\omega)\mathbf{B}^T. \tag{15}$$

where $\mathbf{H}_A$ is a diagonal matrix given by

$$\mathbf{H}_A(\omega) = -\omega^2\left(j\omega\mathbf{C}_a + \mathbf{K}_a\right)\left(-\omega^2\mathbf{M}_a + j\omega\mathbf{C}_a + \mathbf{K}_a\right)^{-1}\mathbf{M}_a \tag{16}$$

Thus, the dynamic stiffness matrix of the controlled structure is equal to the sum of the dynamic stiffness matrix of the host structure and a rank-N_a update representing the feedback action of the absorbers on the host structure. Consequently, the SMW formula (Eq. (12)) can be used to compute the compliance of the controlled structure as

$$\mathbf{H}_c^{-1}(\omega) = \mathbf{H}_0^{-1}(\omega) - \mathbf{H}_0^{-1}(\omega)\mathbf{B}\left(\mathbf{H}_A^{-1}(\omega) + \mathbf{B}^T\mathbf{H}_0^{-1}(\omega)\mathbf{B}\right)^{-1}\mathbf{B}^T\mathbf{H}_0^{-1}(\omega) \tag{17}$$

Eq. (17) can be subject to singularity issues in three cases. The first one is $\omega = 0$, because $\mathbf{H}_A(0)$ is a zero matrix. In that case, Eq. (15) simply indicates that $\mathbf{H}_c^{-1}(0) = \mathbf{H}_0^{-1}(0)$. The second case occurs if any $m_{a,n}$ is zero, or if any pair $(c_{a,n}, k_{a,n})$ is zero. These cases correspond to an absence of absorber or to an unattached absorber mass, which is irrelevant in the design problem. Finally, the SMW formula requires $\mathbf{H}_0$ to be non-singular. This condition might not be met at the resonance frequencies of an undamped host structure. In this case, a small amount of damping may be added to resolve this numerical issue while still representing faithfully the dynamics of the host.

The SMW formula reduces the cost of computing the dynamic stiffness matrix of the controlled structure. Indeed, instead of inverting a system of equations of size $(N + N_a) \times (N + N_a)$ (Eq. (9)),

the SMW formula requires an inversion of a matrix of size $N_a \times N_a$ (Eq. (17)) when $\mathbf{H}_0^{-1}$ is known. Accounting for the additional matrix products, the theoretical complexity of computing the controlled FRF then becomes $O(N^2 N_a + N_a^3)$ instead of $O((N+N_a)^3)$, which is advantageous when $N \gg N_a$.

Finally, the compliance at a given displacement located by a vector $\mathbf{w}_u$, is

$$h(\omega) = \mathbf{w}_u^T \mathbf{H}_c^{-1}(\omega) \mathbf{w}_f, \tag{18}$$

where $\mathbf{w}_f$ is a vector describing the spatial distribution of the forcing vector $\mathbf{F}$, and $\mathbf{H}_c^{-1}$ is evaluated using Eq. (17). Alternatively, the accelerance (i.e., the transfer function between an acceleration of interest and the external forcing amplitude) may be considered simply as

$$h_a(\omega) = -\omega^2 h(\omega) \tag{19}$$

3.3. Peak finding

The resonance frequencies occur at the maximum of the compliance, i.e.,

$$\omega_s = \arg\min_{\omega \in \mathbb{R}} s_1(\omega) = \arg\min_{\omega \in \mathbb{R}} \left(-|h(\omega)|^2 \right), \tag{20}$$

where the square modulus of the complex compliance is used to make the function s_1 smooth with respect to ω. A necessary condition to satisfy this relation is

$$\omega_s : \left. \frac{\partial s_1(\omega)}{\partial \omega} \right|_{\omega=\omega_s} = - \left. \left(\frac{\partial h^*(\omega)}{\partial \omega} h(\omega) + h^*(\omega) \frac{\partial h(\omega)}{\partial \omega} \right) \right|_{\omega=\omega_s} = 0, \tag{21}$$

where the superscript $*$ denotes a complex conjugation. This equation can be solved numerically starting from an initial guess (e.g. Eq. (5)) using either root-finding algorithms (paying attention to the fact that a root might not correspond to a maximum of the compliance) or linesearch algorithms [56]. This procedure yields a set of frequencies ω_i and associated amplitudes noted $|h(j\omega_i)| = |h|_i$ with $i = 1, ..., 2N_a$, assuming there are two peaks per controlled mode, as in the baseline case [6].

A similar procedure for the accelerance consists in finding the roots of

$$\omega_s : \left. \frac{\partial s_2(\omega)}{\partial \omega} \right|_{\omega=\omega_s} = -4\omega^3 |h(j\omega)|^2 - \omega^4 \left. \left(\frac{\partial h^*(\omega)}{\partial \omega} h(\omega) + h^*(\omega) \frac{\partial h(\omega)}{\partial \omega} \right) \right|_{\omega=\omega_s} = 0, \tag{22}$$

3.4. p-norm optimization

The goal of the optimization algorithm is to find the optimal mass, damping and stiffness of the absorbers through the nonlinear programming problem

$$\begin{aligned} \underset{\boldsymbol{\xi}}{\text{minimize}} \quad & f_p(\boldsymbol{\xi}) \\ \text{subject to} \quad & \sum_{n=1}^{N_a} m_{a,n} - m_{\text{Max}} \leq 0 \end{aligned}, \tag{23}$$

where $\boldsymbol{\xi}$ is the vector containing the absorber parameters, and f_p is the p-norm of the vector containing the squared amplitudes of the controlled resonance peaks

$$f_p = \chi \sqrt[p]{\sum_{i=1}^{2N_a} \left(\frac{1}{\chi} |h|_i^2 \right)^p}, \tag{24}$$

The sum considers $2N_a$ peaks by reference to the baseline single-mode case [6]. The user can nonetheless consider a different number of peaks, if an initial guess for the frequency of each of these peaks is given. χ is a normalizing factor, which does not affect the norm and avoids bad numerical conditioning for large p. A typical choice for χ is

$$\chi = \max_{i \in [1, 2N_a]} |h|_i^2 \tag{25}$$

For practical reasons, the total mass of the absorbers should not exceed a maximum m_{Max}, which is translated by the addition of a linear inequality constraint in problem (23). It was generally observed in the literature (e.g. [6, 36]), and by the authors as well, that the mass constraint is usually active in the optimum design. The convergence of the algorithm may thus be accelerated when an equality constraint is imposed.

The gradients of the p-norm are computed analytically in the proposed algorithm. From Eq. (24), the l^{th} element of the gradient of the p-norm with respect to the absorbers parameters is given by

$$\frac{\partial f_p}{\partial \xi_l} = \left(\sum_{i=1}^{2N_a} \left(\frac{1}{\chi} |h|_i^2 \right)^{p-1} \left(\frac{\partial h_i^*}{\partial \xi_l} h_i + h_i^* \frac{\partial h_i}{\partial \xi_l} \right) \right) \left(\sum_{i=1}^{2N_a} \left(\frac{1}{\chi} |h|_i^2 \right)^p \right)^{\frac{1}{p}-1}. \tag{26}$$

There is also an implicit dependency of the resonance frequencies on the absorbers parameters, but it can be shown using the chain rule and the necessary condition for resonance frequencies (Eq. (21))

that this implicit dependency does not affect the gradient. The derivatives of the compliance with respect to ξ_l are computed thanks to Eq. (17) and (18) as

$$\frac{\partial h_i}{\partial \xi_l} = \mathbf{w}_u^T \mathbf{G}(\omega_i) \frac{\partial \mathbf{H}_A^{-1}(\omega_i)}{\partial \xi_l} \mathbf{G}^T(\omega_i) \mathbf{w}_f \tag{27}$$

where ω_i are the solutions of Eq. (21) or Eq. (22), and

$$\mathbf{G}(\omega_i) = \mathbf{H}_0^{-1}(\omega_i)\mathbf{B}\left(\mathbf{H}_A^{-1}(\omega_i) + \mathbf{B}^T\mathbf{H}_0^{-1}(\omega_i)\mathbf{B}\right)^{-1}. \tag{28}$$

Despite the rather complicated structure of Eqs. (27) and (28), computing the gradient of the cost function is not cumbersome for two reasons. First, each element in Eq. (28) is known from the computation of $|h|_i$. Second, the derivative of $\mathbf{H}_A^{-1}$ with respect to ξ_l can be computed analytically and contains only one non-zero entry. Assuming ξ_l is a parameter associated with the n^{th} absorber, the corresponding entry is given by

$$\left(\frac{\partial \mathbf{H}_A^{-1}(\omega_i)}{\partial \xi_l}\right)_{n,n} = \begin{cases} \dfrac{1}{m_{a,n}^2 \omega_i^2} & \text{if } \xi_l = m_{a,n} \\ -\dfrac{j\omega_i}{(k_{a,n} + j\omega_i c_{a,n})^2} & \text{if } \xi_l = c_{a,n} \\ -\dfrac{1}{(k_{a,n} + j\omega_i c_{a,n})^2} & \text{if } \xi_l = k_{a,n} \end{cases} \tag{29}$$

Hence, the gradients of the cost function are obtained analytically by plugging Eq. (29) into Eq. (27) and then into Eq. (26). The gradients of a cost function based on the accelerance are obtained through multiplication by ω_i^4.

The result of the 1-norm optimization of the initial tuning in Fig. 3 is displayed in Fig. 4. The algorithm has thus reduced the initial mistuning.

3.5. Norm-homotopy optimization procedure

Once the optimization has converged for a given value of p, p is then increased in order to penalize high-amplitude peaks more strongly and approach the H_∞ optimum. A heuristic scheme for p given by the double exponential progression

$$p = 2^{2^k}, \qquad k \in \mathbb{N}. \tag{30}$$

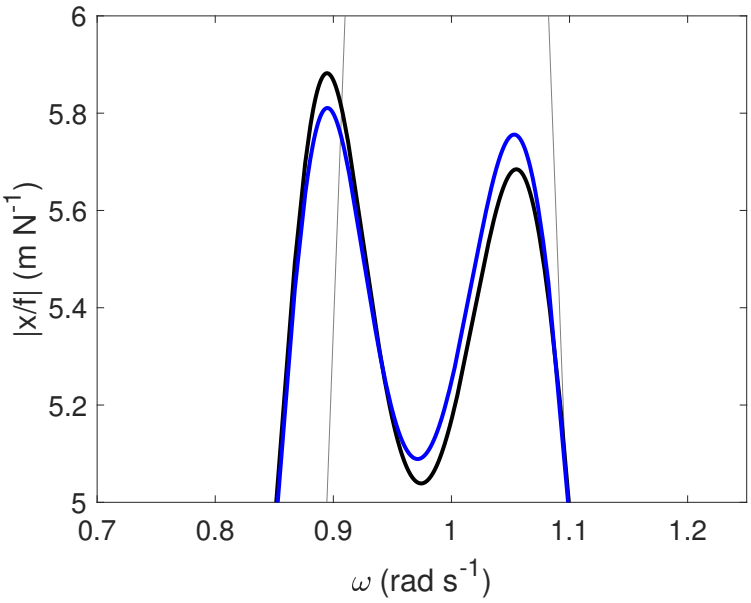

Figure 4: Compliance of the damped single-degree-of-freedom system: uncontrolled structure (—), initial tuning (—) and p-norm optimization with $p = 1$ (—).

is considered. The value of k starts from zero and is incremented by one after convergence. This norm-homotopy algorithm may be terminated when no significant change is observed in the absorbers parameters and/or in the value of the p-norm.

The end result of the norm-homotopy procedure applied to the single-degree-of-freedom system is shown in Fig. 5. The optimization was stopped when k was equal to 4 (i.e., p was equal to 65536). The peaks are now equal.

3.6. Summary

The proposed algorithm is summarized schematically in Fig. 6.

Two remarks are outlined to close this section. First, the compliance and accelerance were used throughout this work in the cost function of the optimization algorithm, but other transfer functions such as mobility could easily be considered as well. Second, only one input-output pair was taken into account (through the vectors $\mathbf{w}_u$ and $\mathbf{w}_f$) for this transfer function for simplicity; more elaborate cost functions than that given in Eq. (24) could be conceived to generalize the approach to multiple inputs and/or outputs (see e.g. [47]).

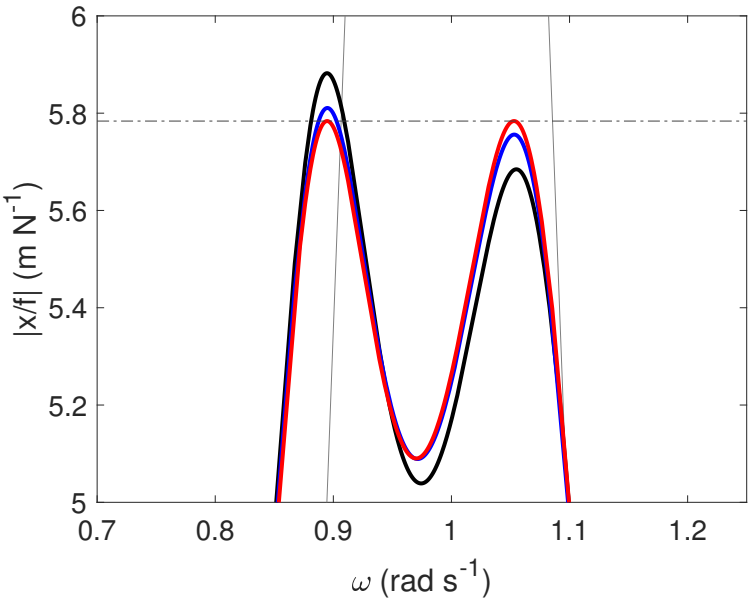

Figure 5: TMD on a damped single-degree-of-freedom system: uncontrolled structure (—), initial tuning (—), p-norm optimization with $p = 1$ (—) and norm-homotopy optimization (—).

4. Examples

Two examples serve to demonstrate the algorithm in this section. The maximum allowable mass for the absorbers is set to 5% of that of the host structure. The optimization problem (23) is solved in MATLAB thanks to the `fmincon` routine. This routine is called for each p-norm optimization step with an initial guess given by the optimal solution computed by the previous p-norm optimization (except for the first optimization, where the initial guess is formed using Equations (3) and (4)). Each time the cost function is called, the peak-finding algorithm solves Eqs. (20)-(21) using a linesearch approach, as described in [56].

The results of the proposed approach were compared with those of a direct H_∞ optimization. The H_∞ norm was computed using a standard method [57]. CPU times were also measured (the PC on which these computations were made has a processor Intel Core i7-7820HQ CPU @ 2.90 GHz and 16 GB of RAM).

4.1. A two-degree-of-freedom host structure

The two-degree-of-freedom structure with the two attached absorbers is depicted in Fig. 7. The parameters of the host system are listed in Table 1. The first absorber, labelled "1" in Fig. 7, targets the first mode whereas the second absorber targets the second mode.

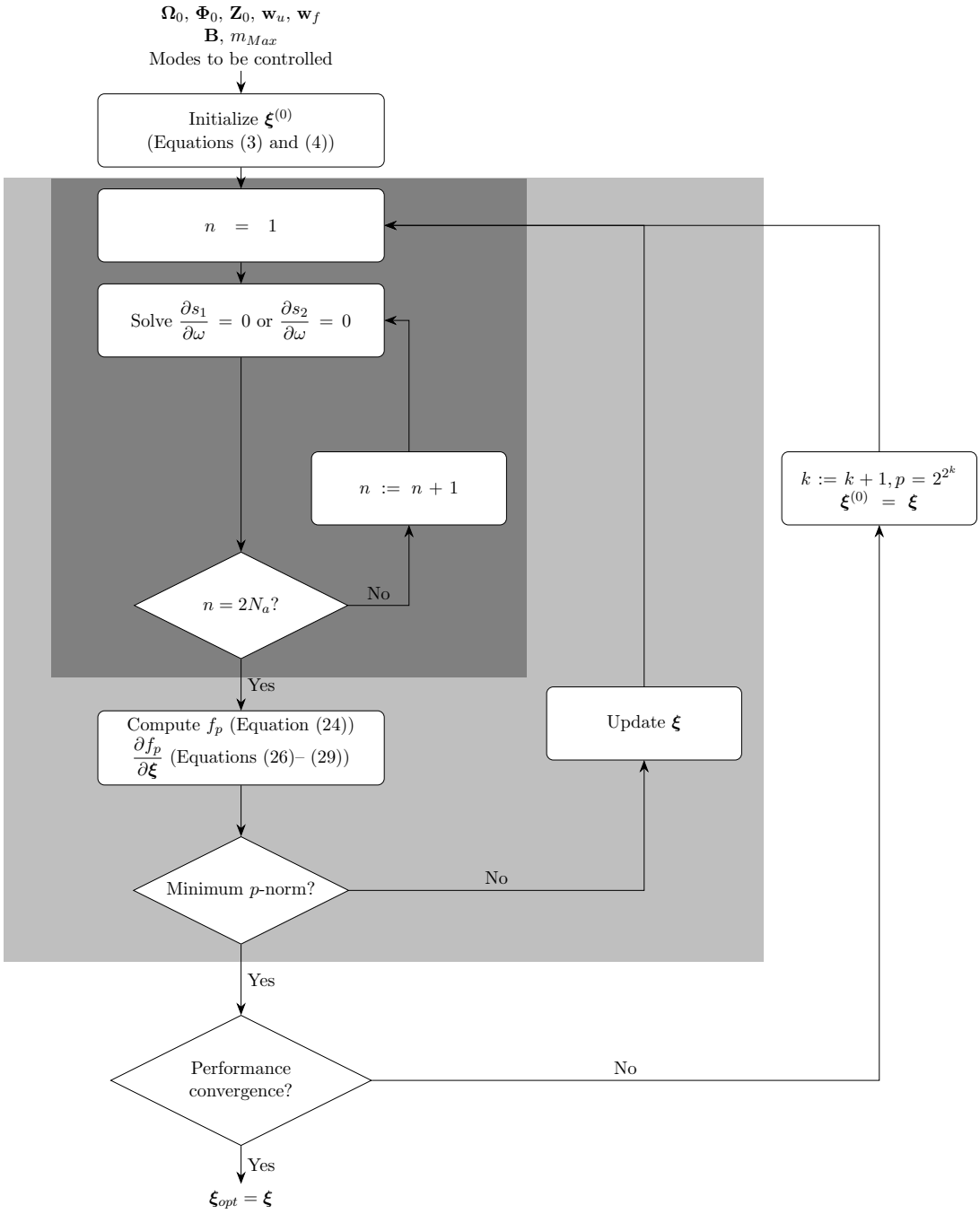

Figure 6: Flowchart of the norm-homotopy optimization algorithm; the dark gray area represents the peak-finding algorithm, and the pale gray area represents the p-norm optimization algorithm.

Fig. 8 displays the compliance of the host structure for different values of k. The initial tuning (whose associated parameters are listed in Table 2) is clearly unsatisfactory, mostly because of the cross-influence between both absorbers. After the optimization for $k = 0$, almost equal peaks

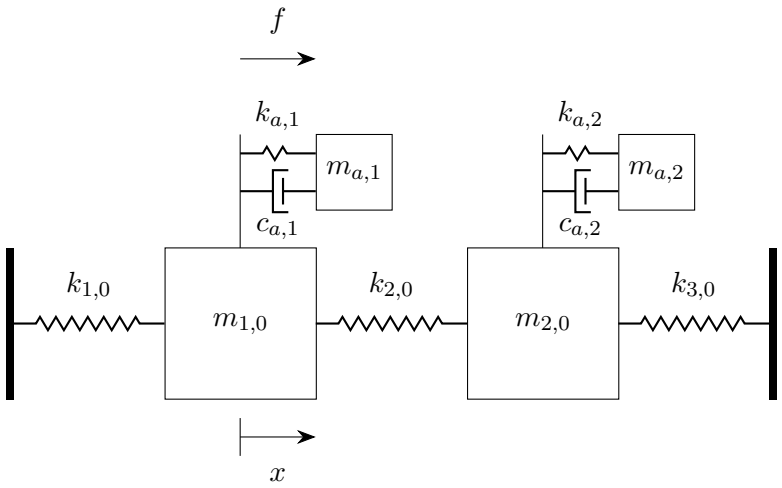

Figure 7: Schematic representation of the two-degree-of-freedom structure with the two attached absorbers.

Parameter	$m_{1,0}$ (kg)	$m_{2,0}$ (kg)	$k_{1,0}$ (N m^{-1})	$k_{2,0}$ (N m^{-1})	$k_{3,0}$ (N m^{-1})
Value	1	1	1	1	1

Table 1: Parameters of the two-degree-of-freedom host structure.

around the two resonances are retrieved, but the amplitude of the peaks around the first mode is still significantly larger than that around the second mode. Increasing k up to 4 eventually leads to the so-called all-equal-peak design. The optimal parameters of the absorbers are listed in Table 3. In this case, the results were identical to those given by a direct H_∞ optimization.

Parameter	m_a (kg)	c_a (N s m^{-1})	k_a (N m^{-1})
Absorber 1	$0.5m_{\mathrm{Max}}$	0.0093	0.0476
Absorber 2	$0.5m_{\mathrm{Max}}$	0.0162	0.1428

Table 2: Initial parameters of the absorbers in Fig. 7 for compliance optimization.

Parameter	m_a (kg)	c_a (N s m^{-1})	k_a (N m^{-1})
Absorber 1	$0.94m_{\mathrm{Max}}$	0.0237	0.0840
Absorber 2	$0.06m_{\mathrm{Max}}$	0.0007	0.0183

Table 3: Optimal parameters of the absorbers in Fig. 7 for compliance optimization.

4.1.1. Computational cost

To make a first assessment of the approach proposed in this paper, three different optimization approaches are compared, namely the norm-homotopy optimization using the SMW formula, the norm-homotopy optimization without SMW formula and a direct H_∞ optimization. The three

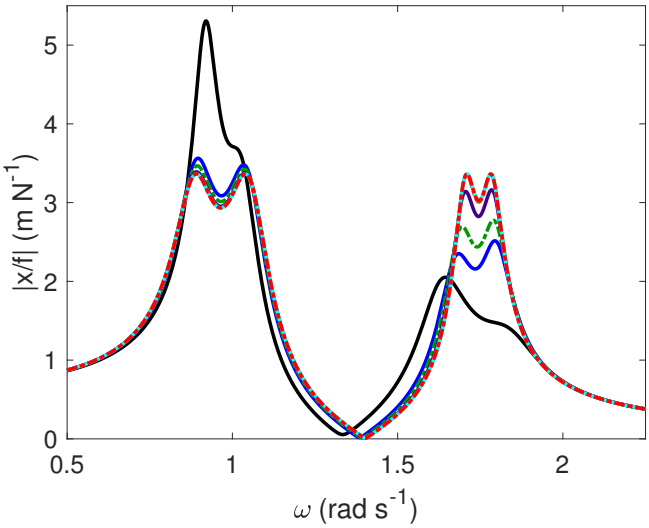

Figure 8: MTMD on a two-degree-of-freedom system: initial tuning (—), solution for $k = 0$ (—), solution for $k = 1$ (-·-), solution for $k = 2$ (—), solution for $k = 3$ (-·-), solution for $k = 4$ (—), and norm-homotopy optimal solution (-·-).

approaches yielded identical optimal results, and are compared here in terms of runtimes. Table 4 gives the CPU times (averaged over 50 optimizations of each type). It indicates that the SMW formula offers a slight speedup in spite of the low number of variables. A direct H_∞ optimization is nonetheless the fastest approach in this case.

Case	t_f	t_{Tot}	t_0	t_1	t_2	t_3	t_4	t_5
NH, SMW	0.0027	1.4563	0.2038	0.2841	0.1792	0.2567	0.3747	0.1556
NH, no SMW	0.0035	1.8756	0.2596	0.3680	0.2404	0.3412	0.4684	0.1977
H_∞	0.0024	1.0427	/	/	/	/	/	/

Table 4: CPU times (in s) of the different optimizations of two absorbers (NH stands for norm-homotopy optimization, H_∞ stands for direct H_∞ optimization, t_f is average time per cost function evaluation, t_{Tot} is the average total runtime, t_k is the average time spent for a p-norm optimization with a specific value of k (Equation (30)) in the NH case).

4.1.2. Accelerance optimization

Figure 9 shows the results of a norm-homotopy optimization on the accelerance, and Table 5 gives the corresponding optimal characteristics. Again, peaks of equal amplitude are observed, which illustrates the versatility of the approach.

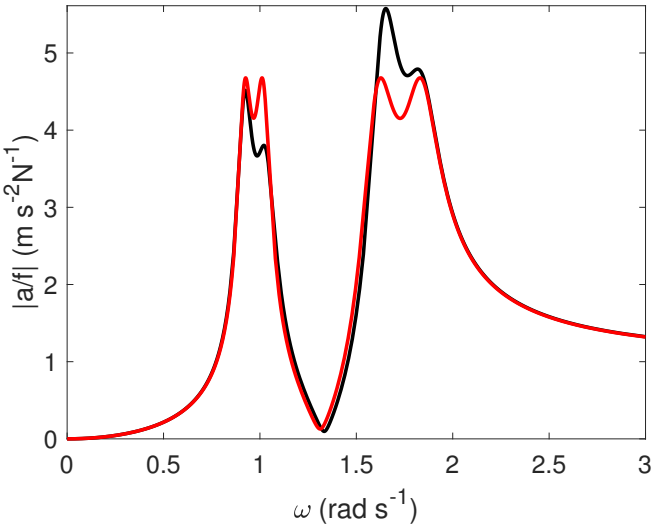

Figure 9: MTMD on a two-degree-of-freedom system: initial tuning (—), and norm-homotopy optimal solution (—).

Parameter	m_a (kg)	c_a (N s m^{-1})	k_a (N m^{-1})
Absorber 1	$0.37m_{\text{Max}}$	0.0057	0.0342
Absorber 2	$0.63m_{\text{Max}}$	0.0213	0.1720

Table 5: Optimal parameters of the absorbers in Fig. 7 for accelerance optimization.

4.2. A simply-supported aluminum plate

The second example is a homogeneous, isotropic, simply-supported rectangular plate that features closely-spaced resonances. According to Kirchhoff-Love theory, the mode shapes and eigenfrequencies of a plate of length a, width b and thickness h are given by

$$\begin{aligned} \phi_{mn}(x,y) &= \frac{2}{\sqrt{M}} \sin\left(\frac{m\pi x}{a}\right) \sin\left(\frac{n\pi y}{b}\right) \\ \omega_{mn} &= \sqrt{\frac{D}{\rho h}} \left[\left(\frac{m\pi}{a}\right)^2 + \left(\frac{n\pi}{b}\right)^2 \right] \end{aligned} , \tag{31}$$

respectively [52]. ρ is the density of the plate, $M = \rho abh$ is the mass of the plate, and $D = Eh^3/(12(1-\nu^2))$ is the plate bending stiffness, where E and ν are Young's modulus Poisson's ratio, respectively. The plate parameters are given in Table 6.

To discretize the model, the mode shapes are sampled spatially at locations $(\mathbf{x}_s, \mathbf{y}_s)$, where

$$\begin{aligned} \mathbf{x}_s &= [x_u, x_{a,1}, x_{a,2}, x_{a,3}, x_{a,4}, x_f]^T &= [0.25a, 0.5a, 0.15a, 0.4a, 0.25a, 0.75a]^T \\ \mathbf{y}_s &= [y_u, y_{a,1}, y_{a,2}, y_{a,3}, y_{a,4}, y_f]^T &= [0.25b, 0.5b, 0.4b, 0.15b, 0.75b, 0.75b]^T \end{aligned} , \tag{32}$$

and only a finite number of modes is retained, up to $m = M_{\text{Max}} = 10$ and $n = N_{\text{Max}} = 10$. The mode shape matrix of the host structure and the matrix of squared resonance frequencies are

Characteristic	Value
Length a	1 m
Width b	0.7 m
Thickness h	1 mm
Young modulus E	68 GPa
Poisson ratio ν	0.36
Density ρ	2700 kg m^{-3}

Table 6: Parameters of the simply-supported aluminum plate.

ordered such that

$$\mathbf{\Phi}_0 = \left[\phi_{11}(\mathbf{x}_s, \mathbf{y}_s), \phi_{12}(\mathbf{x}_s, \mathbf{y}_s), \cdots, \phi_{M_{\text{Max}}N_{\text{Max}}}(\mathbf{x}_s, \mathbf{y}_s)\right], \tag{33}$$

$$\mathbf{\Omega}_0^2 = \text{diag}\left(\omega_{11}^2, ..., \omega_{M_{\text{Max}}N_{\text{Max}}}^2\right). \tag{34}$$

The plate is loaded by a harmonic point force located at (x_f, y_f). Three/four absorbers are considered to mitigate the first three/four resonances, respectively. Fig. 10 depicts the geometrical configuration. The first and fourth TMDs were placed at an antinode of the first and fifth modes, associated to $(m, n) = (1, 1)$ and $(m, n) = (2, 2)$, respectively, to maximize their effect on these modes. The second and third TMDs were placed away from the nodal lines of modes for which $n = 2$ or $m = 2$, but not at their antinodes in order to affect higher-frequency modes as well. The forcing and displacement measurement locations were chosen arbitrarily, away from the TMDs and in a non-collocated fashion to contrast with the previously studied example.

To have a numerically well-conditioned problem, the compliance measured at coordinates (x_u, y_u) is normalized with the static displacement x_{st} of the structure

$$x_{\text{st}}(x_u, y_u) = \sum_{m=1}^{M_{\text{Max}}} \sum_{n=1}^{N_{\text{Max}}} \frac{\phi_{mn}(x_u, y_u)\phi_{mn}(x_f, y_f)}{\omega_{mn}^2} f. \tag{35}$$

4.2.1. Vibration mitigation with three absorbers

The first three modes, i.e., $(m, n) = (1, 1)$, $(2, 1)$ and $(1, 2)$, are first targeted. The result of the H_∞ optimization (limiting the range of frequencies up to $\omega = 150$ rad s^{-1}) and the norm-homotopy optimization are presented in Fig. 11, and Table 7 lists the parameters of the resulting absorbers. Although it shows improvement with respect to the initial tuning, the direct H_∞ norm optimization stops somewhat prematurely, and only four peaks are equated in amplitude. With the norm-homotopy optimization, the six peaks around the first three resonances all feature the same amplitude, which further validates the proposed methodology.

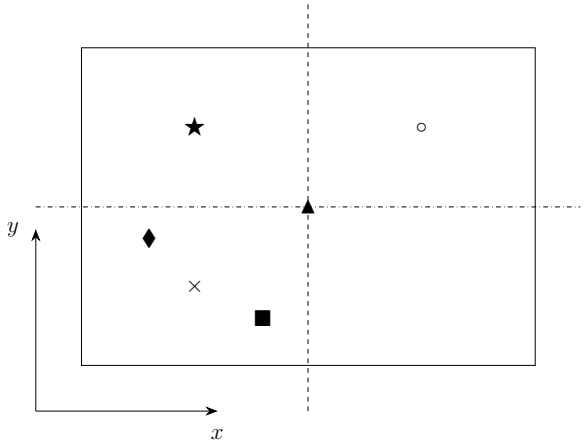

Figure 10: Geometry of the plate: point force location (×), displacement measurement location (○), first TMD location (▲), second TMD location (♦), third TMD location (■), fourth TMD location (★), nodal line of modes for which $m = 2$ (- -) and nodal line of modes for which $n = 2$ (– · –).

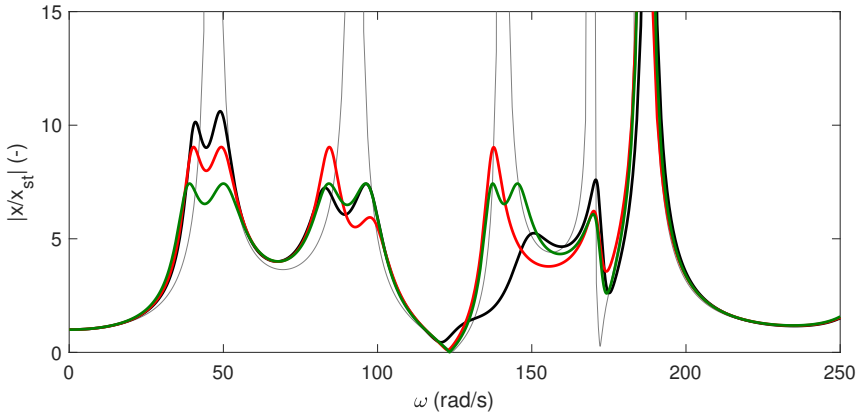

Figure 11: Compliance of the plate with three absorbers targeting modes $(1,1)$, $(2,1)$ and $(1,2)$: uncontrolled structure (—), initial tuning (—) and optimized tuning (—: direct H_∞ optimization, —: norm-homotopy optimization).

Absorber number	m_a (kg)	c_a (N s m^{-1})	k_a (N m^{-1})
1	$0.65m_{\text{Max}}$	1.1348	110.42
2	$0.3m_{\text{Max}}$	0.6044	225.36
3	$0.05m_{\text{Max}}$	0.0666	94.93

Table 7: Parameters of the three absorbers.

4.2.2. Vibration mitigation with four absorbers

In the previous example, the fifth mode of the plate remained largely unaffected (whereas the fourth mode was mitigated). To improve the situation, a fourth absorber targeting this mode is placed on the plate. Fig. 12 displays the result of the optimization processes (where a maximum frequency of $\omega = 250$ rad s^{-1} was considered when computing the H_∞ norm). The direct H_∞

norm optimization only features marginal improvement compared to the initial design. The norm-homotopy optimization obeys the all-equal-peak design and has a lower H_∞ norm, in the considered frequency range. However, we note that modes 3, 4 and 5 do not feature two peaks around their uncontrolled resonance. Looking at the absorber parameters in Table 8 reveals that the third absorber is in fact eliminated by the optimization algorithm (zero mass), while modes 3-5 are controlled by an action of the three TMDs simultaneously. This result probably originates from the fact that plates have closely-spaced frequencies, and the peak-finding algorithm described in Section 3.3 finds the peak associated to mode 4 starting from the assumed first peak frequency of mode 5.

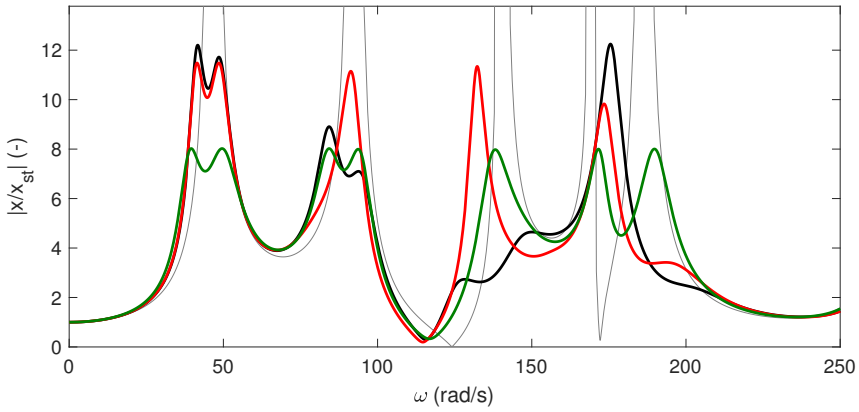

Figure 12: Compliance of the plate with four absorbers targeting modes $(1,1)$, $(2,1)$, $(1,2)$ and $(2,2)$: uncontrolled structure (—), initial tuning (—) and optimized tuning (—: direct H_∞ optimization, —: norm-homotopy optimization).

Absorber number	m_a (kg)	c_a (N s m^{-1})	k_a (N m^{-1})
1	$0.56m_{\text{Max}}$	0.9074	96.0221
2	$0.22m_{\text{Max}}$	0.3665	164.7649
3	$1\times10^{-7}m_{\text{Max}}$	67.1701	442.2204
4	$0.22m_{\text{Max}}$	1.0619	444.1343

Table 8: Parameters of the four absorbers.

An additional configuration was considered where TMDs 2 to 4 were placed on a nodal line of mode 4, i.e., by changing their x coordinate in Eq. (32) to $a/3$. For this configuration, the result featured in Fig. 13 is more in line with the expectation: each controlled mode features a pair of peaks of equal amplitude. The associated parameters are given in Table 9. This result shows that a significant part of the observed vibration reduction of mode 4 is due to the first TMD, but the third

TMD also played a role in reducing the amplitude of this mode. It also highlights the importance of the absorbers positions, which could be an interesting aspect to integrate in the optimization, but is beyond the scope of the present work.

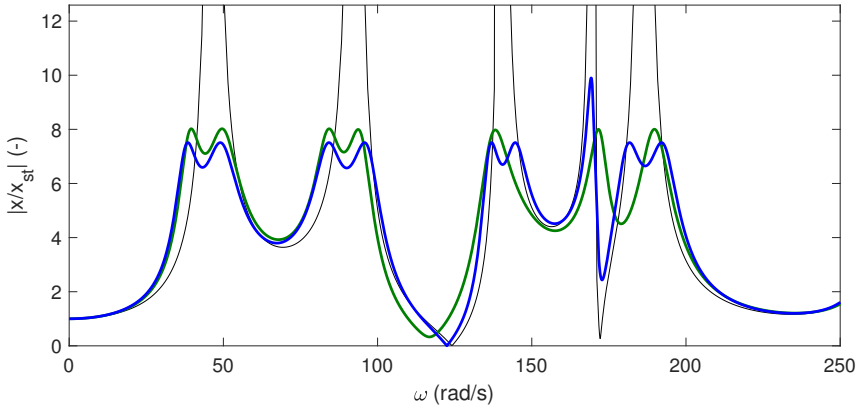

Figure 13: Compliance of the plate with four absorbers targeting modes $(1,1)$, $(2,1)$, $(1,2)$ and $(2,2)$: uncontrolled structure (—) and optimized tuning with norm-homotopy optimization using the TMDs positions depicted in Fig. 10 (—) and placing TMDs 2-4 on the nodal line of mode 4 (—).

Absorber number	m_a (kg)	c_a (N s m^{-1})	k_a (N m^{-1})
1	$0.64m_{\text{Max}}$	1.0663	105.5866
2	$0.26m_{\text{Max}}$	0.4858	188.7259
3	$0.05m_{\text{Max}}$	0.0669	99.1084
4	$0.04m_{\text{Max}}$	0.0739	136.6114

Table 9: Parameters of the four absorbers (with TMDs 2-4 on the nodal line of mode 4).

4.2.3. Computational cost

Using the same three optimization approaches as in Subsection 4.1.1, the two cases of the plate with three and four absorbers can be compared in terms of CPU times (averaged over 10 optimizations) in Tables 10 and 11, respectively. These tables highlight the computational advantage of the SMW formula, with which both the time to evaluate the cost function and the total runtime are decreased by two orders of magnitude. The norm-homotopy approach (with and without SMW formula) requires more cost function evaluations, but converges to a solution with a lower H_∞ norm than the direct H_∞ optimization.

4.2.4. Design robustness

In real-life applications, the model parameters may be known with limited accuracy. For illustration, variations of $\pm 5\%$ of Young's modulus are presented herein, while every other parameter is

Case	t_f	t_{Tot}	t_0	t_1	t_2	t_3	t_4	t_5
NH, SMW	0.0050	4.7483	0.8229	0.6875	0.6771	0.8472	1.4826	0.2309
NH, no SMW	0.58112	490.83	95.29	77.62	66.77	83.69	130.34	37.12
H_∞	1.3951	232.97	/	/	/	/	/	/

Table 10: CPU times (in s) of the different optimizations of three absorbers (NH stands for norm-homotopy optimization, H_∞ stands for direct H_∞ optimization, t_f is average time per cost function evaluation, t_{Tot} is the average total runtime, t_k is the average time spent for a p-norm optimization with a specific value of k (Equation (30)) in the NH case).

Case	t_f	t_{Tot}	t_0	t_1	t_2	t_3	t_4	t_5
NH, SMW	0.0070	7.2431	2.4688	2.0972	0.9080	1.3368	0.1372	0.2951
NH, no SMW	0.8599	1053.91	104.80	159.68	258.97	160.83	303.34	66.30
H_∞	1.7156	187.00	/	/	/	/	/	/

Table 11: CPU times (in s) of the different optimizations of four absorbers (NH stands for norm-homotopy optimization, H_∞ stands for direct H_∞ optimization, t_f is average time per cost function evaluation, t_{Tot} is the average total runtime, t_k is the average time spent for a p-norm optimization with a specific value of k (Equation (30)) in the NH case).

kept constant. The absorbers parameters of Table 8 are used. As depicted in Fig. 14, the absorbers are detuned in a fashion similar to that of the single-degree-of-freedom case, and an increase in the maximum amplification of 15% (-5% case) and 27% (5% case) can be noticed.

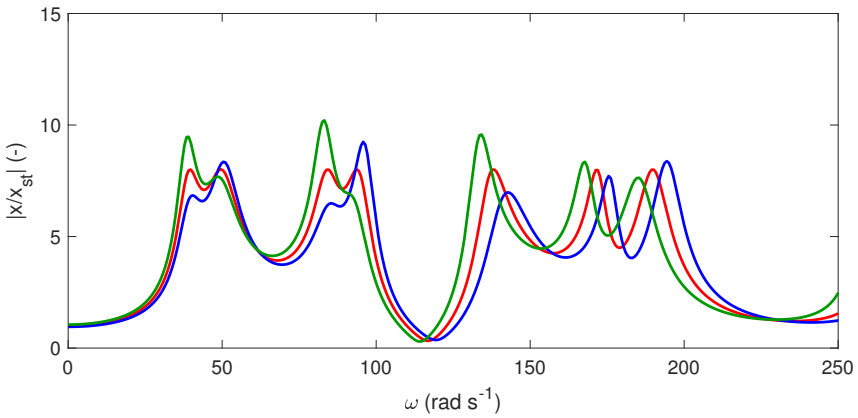

Figure 14: Design robustness: nominal value of E (—), 5% increase (—) and 5% decrease (—).

5. Conclusion

A norm-homotopy numerical optimization algorithm was proposed in this paper to tune multiple TMDs targeting several resonances of a host structure. The algorithm solves a sequence of optimization problems of increasing complexity in which the cost function depends on the p-norm

of the peak amplitudes of the compliance/accelerance of the controlled structure. The value of p is controlled by increments of a parameter k. Small values of k (or p) are associated with an optimization problem with a smoother objective function than the H_∞ norm, thereby easing convergence. High values of k (or p) are used at the end of the algorithm to make the optimization problem close to a H_∞ one. As demonstrated by the examples, the outcome of the algorithm is an all-equal-peak design, in which all controlled peaks feature the same amplitude. The algorithm can deal with a variety of discretized structures with moderate computational cost and was also found to outperform direct H_∞ optimization. Specifically, the norm-homotopy approach enabled the optimizer to reach a lower H_∞ norm, and the use of the SMW formula speeded up the optimization. The norm-homotopy approach does not have a theoretical guarantee to reach the global minimum of the H_∞ norm, but the all-equal-peak outcome appears as a satisfactory local optimum.

Future works may adapt the algorithm to other types of absorbers (e.g., nonlinear absorbers) and may involve the experimental validation of the proposed design approach. The position of the absorbers on the structure could also be considered as optimization variables in the method.

Acknowledgements

Funding: This work was supported by the SPW [WALInnov grant 1610122].

Appendix A. Single TMD on a multiple-degree-of-freedom structure

It is considered that only the n^{th} absorber is attached to the host structure. Around its resonance frequency ω_n, it can be assumed that a resonant mode n dominates the structural response. Thus, the following relation approximately holds for $\omega \approx \omega_n$

$$\begin{bmatrix} \mathbf{X}(\omega) \\ X_{a,n}(\omega) \end{bmatrix} = \begin{bmatrix} \boldsymbol{\phi}_n & \mathbf{0} \\ 0 & 1 \end{bmatrix} \begin{bmatrix} \eta_n(\omega) \\ X_{a,n}(\omega) \end{bmatrix} = \mathbf{A}_n \begin{bmatrix} \eta_n(\omega) \\ X_{a,n}(\omega) \end{bmatrix}, \tag{A.1}$$

where $\boldsymbol{\phi}_n$ is the mass-normalized resonant mode shape, η_n is the associated resonant modal coordinate and $X_{a,n}$ is the generalized degree of freedom associated with the n^{th} absorber. Substituting Eq. (A.1) into Eq. (9) (where only the n^{th} absorber is considered), premultiplying it by $\mathbf{A}_n^T$ and

taking into account the modal orthogonality relationships [52], one gets

$$\left(-\omega^2\begin{bmatrix}1 & 0\\ 0 & m_{a,n}\end{bmatrix}+j\omega\begin{bmatrix}2\zeta_n\omega_n+\phi_{a,n}^2c_{a,n} & -\phi_{a,n}c_{a,n}\\ -\phi_{a,n}c_{a,n} & c_{a,n}\end{bmatrix}+\begin{bmatrix}\omega_n^2+\phi_{a,n}^2k_{a,n} & -\phi_{a,n}k_{a,n}\\ -\phi_{a,n}k_{a,n} & k_{a,n}\end{bmatrix}\right)\begin{bmatrix}\eta_n(\omega)\\ X_{a,n}(\omega)\end{bmatrix}=\begin{bmatrix}\boldsymbol{\phi}_n^T\mathbf{F}(\omega)\\ 0\end{bmatrix}, \tag{A.2}$$

where ζ_n is the n^{th} modal damping ratio and $\phi_{a,n}=\mathbf{b}_n^T\boldsymbol{\phi}_n$ is the mode shape of the host structure at the location where the absorber is to be attached. The base displacement of the n^{th} absorber U_n is given by

$$U_n(\omega)=\mathbf{b}_n^T\mathbf{X}(\omega)=\mathbf{b}_n^T\boldsymbol{\phi}_n\eta_n(\omega)=\phi_{a,n}\eta_n(\omega). \tag{A.3}$$

Inserting Eq. (A.3) into Eq. (A.2) and multiplying the first line of the latter by $1/\phi_{a,n}$, one obtains

$$\left(-\omega^2\begin{bmatrix}\frac{1}{\phi_{a,n}^2} & 0\\ 0 & m_{a,n}\end{bmatrix}+j\omega\begin{bmatrix}2\zeta_n\frac{\omega_n}{\phi_{a,n}^2}+c_{a,n} & -c_{a,n}\\ -c_{a,n} & c_{a,n}\end{bmatrix}+\begin{bmatrix}\frac{\omega_n^2}{\phi_{a,n}^2}+k_{a,n} & -k_{a,n}\\ -k_{a,n} & k_{a,n}\end{bmatrix}\right)\begin{bmatrix}U_n(\omega)\\ X_{a,n}(\omega)\end{bmatrix}=\begin{bmatrix}\frac{\boldsymbol{\phi}_n^T\mathbf{F}(\omega)}{\phi_{a,n}}\\ 0\end{bmatrix} \tag{A.4}$$

which has the same form as the equations of motions of a single-degree-of-freedom oscillator to which an absorber is attached. Warburton [5] arrived to the same conclusion using energy considerations.

References

[1] H. Frahm, Device for damping vibrations of bodies. (1911).
URL https://patents.google.com/patent/US989958A/en

[2] J. Ormondroyd, J. Den Hartog, Theory of the dynamic vibration absorber, J. Appl. Mech. 50 (7) (1928) 11–22.

[3] J. E. Brock, A note on the damped vibration absorber, Trans. ASME, J. Appl. Mech. 13 (4) (1946) A—-284.

[4] J. P. Den Hartog, Mechanical vibrations, Courier Corporation, 1985.

[5] G. B. Warburton, Optimum absorber parameters for various combinations of response and excitation parameters, Earthq. Eng. Struct. Dyn. 10 (3) (1982) 381–401. doi:10.1002/eqe.4290100304.
URL http://doi.wiley.com/10.1002/eqe.4290100304

[6] O. Nishihara, T. Asami, Closed-Form Solutions to the Exact Optimizations of Dynamic Vibration Absorbers (Minimizations of the Maximum Amplitude Magnification Factors), J. Vib. Acoust. 124 (4) (2002) 576. doi:10.1115/1.1500335.
URL http://vibrationacoustics.asmedigitalcollection.asme.org/article.aspx?articleid=1470453

[7] M. Gutierrez Soto, H. Adeli, Tuned Mass Dampers, Archives of Computational Methods in Engineering 20 (4) (2013) 419–431. doi:10.1007/s11831-013-9091-7.
URL http://link.springer.com/10.1007/s11831-013-9091-7

[8] S. Elias, V. Matsagar, Research developments in vibration control of structures using passive tuned mass dampers, Annu. Rev. Control 44 (2017) 129–156. doi:10.1016/j.arcontrol.2017.09.015.
URL https://linkinghub.elsevier.com/retrieve/pii/S1367578817301372

[9] M. De Angelis, S. Perno, A. Reggio, Dynamic response and optimal design of structures with large mass ratio TMD, Earthquake Engineering & Structural Dynamics 41 (1) (2012) 41–60. doi:10.1002/eqe.1117.
URL http://doi.wiley.com/10.1002/eqe.1117

[10] D. De Domenico, G. Ricciardi, An enhanced base isolation system equipped with optimal tuned mass damper inerter (TMDI), Earthquake Engineering & Structural Dynamics 47 (5) (2018) 1169–1192. doi:10.1002/eqe.3011.
URL http://doi.wiley.com/10.1002/eqe.3011

[11] L. Dell'Elce, E. Gourc, G. Kerschen, A robust equal-peak method for uncertain mechanical systems, J. Sound Vib. 414 (2018) 97–109. doi:10.1016/j.jsv.2017.10.038.
URL https://linkinghub.elsevier.com/retrieve/pii/S0022460X17307629

[12] G. Habib, T. Detroux, R. Viguié, G. Kerschen, Nonlinear generalization of Den Hartog's equal-peak method, Mech. Syst. Signal Process. 52-53 (1) (2015) 17–28. arXiv:arXiv:1604.03868v1, doi:10.1016/j.ymssp.2014.08.009.
URL http://dx.doi.org/10.1016/j.ymssp.2014.08.009

[13] J. C. Snowdon, SteadyState Behavior of the Dynamic AbsorberAddendum, J. Acoust. Soc. Am. 36 (6) (1964) 1121–1123. doi:10.1121/1.1919171.
URL http://asa.scitation.org/doi/10.1121/1.1919171

[14] K. Iwanami, K. Seto, An Optimum Design Method for the Dual Dynamic Damper and its Effectiveness, Bull. JSME 27 (231) (1984) 1965–1973. doi:10.1299/jsme1958.27.1965.
URL http://joi.jlc.jst.go.jp/JST.Journalarchive/jsme1958/27.1965?from=CrossRef

[15] T. Igusa, K. Xu, Vibration Control Using Multiple Tuned Mass Dampers, J. Sound Vib. 175 (4) (1994) 491–503. doi:10.1006/jsvi.1994.1341.
URL https://linkinghub.elsevier.com/retrieve/pii/S0022460X84713411

[16] H. Yamaguchi, N. Harnpornchai, Fundamental characteristics of Multiple Tuned Mass Dampers for suppressing harmonically forced oscillations, Earthq. Eng. Struct. Dyn. 22 (1) (1993) 51–62. doi:10.1002/eqe.4290220105.
URL http://doi.wiley.com/10.1002/eqe.4290220105

[17] M. Abé, Y. Fujino, Dynamic characterization of multiple tuned mass dampers and some design formulas, Earthq. Eng. Struct. Dyn. 23 (8) (1994) 813–835. doi:10.1002/eqe.4290230802.
URL http://doi.wiley.com/10.1002/eqe.4290230802

[18] V. H. Neubert, Dynamic Absorbers Applied to a Bar That Has Solid Damping, J. Acoust. Soc. Am. 36 (4) (1964) 673–680. doi:10.1121/1.1919039.
URL http://asa.scitation.org/doi/10.1121/1.1919039

[19] J. C. Snowdon, Vibration of Cantilever Beams to which Dynamic Absorbers are Attached, J. Acoust. Soc. Am. 39 (5A) (1966) 878–886. doi:10.1121/1.1909966.
URL http://asa.scitation.org/doi/10.1121/1.1909966

[20] L. Kitis, B. Wang, W. Pilkey, Vibration reduction over a frequency range, J. Sound Vib. 89 (4) (1983) 559–569. doi:10.1016/0022-460X(83)90357-7.
URL https://linkinghub.elsevier.com/retrieve/pii/0022460X83903577

[21] H. Özgüven, B. Çandir, Suppressing the first and second resonances of beams by dynamic vibration absorbers, J. Sound Vib. 111 (3) (1986) 377–390. doi:10.1016/S0022-460X(86)81399-2.
URL https://linkinghub.elsevier.com/retrieve/pii/S0022460X86813992

[22] R. Rana, T. Soong, Parametric study and simplified design of tuned mass dampers, Eng. Struct. 20 (3) (1998) 193–204. doi:10.1016/S0141-0296(97)00078-3.
URL https://linkinghub.elsevier.com/retrieve/pii/S0141029697000783

[23] A. J. Clark, Multiple passive tuned mass damper for reducing earthquake induced building motion, in: 9th World Conf. Earthq. Eng., 1988, pp. 779–784.

[24] J.-D. Yau, Y.-B. Yang, A wideband MTMD system for reducing the dynamic response of continuous truss bridges to moving train loads, Eng. Struct. 26 (12) (2004) 1795–1807. doi:10.1016/j.engstruct.2004.06.015.
URL https://linkinghub.elsevier.com/retrieve/pii/S0141029604001993

[25] S. Krenk, J. Høgsberg, Tuned resonant mass or inerter-based absorbers: unified calibration with quasi-dynamic flexibility and inertia correction, Proc. R. Soc. A Math. Phys. Eng. Sci. 472 (2185) (2016) 20150718. doi:10.1098/rspa.2015.0718.
URL http://rspa.royalsocietypublishing.org/lookup/doi/10.1098/rspa.2015.0718

[26] C. Li, W. Qu, Optimum properties of multiple tuned mass dampers for reduction of translational and torsional response of structures subject to ground acceleration, Eng. Struct. 28 (4) (2006) 472–494. doi:10.1016/j.engstruct.2005.09.003.
URL https://linkinghub.elsevier.com/retrieve/pii/S0141029605003196

[27] B. Han, C. Li, Characteristics of linearly distributed parameter-based multiple-tuned mass dampers, Struct.

Control Heal. Monit. 15 (6) (2008) 839–856. doi:10.1002/stc.222.
URL http://doi.wiley.com/10.1002/stc.222

[28] D. A. Rade, V. Steffen, OPTIMISATION OF DYNAMIC VIBRATION ABSORBERS OVER A FREQUENCY BAND, Mech. Syst. Signal Process. 14 (5) (2000) 679–690. doi:10.1006/mssp.2000.1319.
URL https://linkinghub.elsevier.com/retrieve/pii/S0888327000913190

[29] L. Zuo, S. Nayfeh, Minimax optimization of multi-degree-of-freedom tuned-mass dampers, J. Sound Vib. 272 (3-5) (2004) 893–908. doi:10.1016/S0022-460X(03)00500-5.
URL https://linkinghub.elsevier.com/retrieve/pii/S0022460X03005005

[30] N. Hoang, P. Warnitchai, Design of multiple tuned mass dampers by using a numerical optimizer, Earthq. Eng. Struct. Dyn. 34 (2) (2005) 125–144. doi:10.1002/eqe.413.
URL http://doi.wiley.com/10.1002/eqe.413

[31] H.-N. Li, X.-L. Ni, Optimization of non-uniformly distributed multiple tuned mass damper, J. Sound Vib. 308 (1-2) (2007) 80–97. doi:10.1016/j.jsv.2007.07.014.
URL https://linkinghub.elsevier.com/retrieve/pii/S0022460X07005561

[32] J. Salvi, E. Rizzi, Optimum tuning of Tuned Mass Dampers for frame structures under earthquake excitation, Structural Control and Health Monitoring 22 (4) (2015) 707–725. doi:10.1002/stc.1710.
URL http://doi.wiley.com/10.1002/stc.1710

[33] D. De Domenico, G. Ricciardi, Optimal design and seismic performance of tuned mass damper inerter (TMDI) for structures with nonlinear base isolation systems, Earthquake Engineering & Structural Dynamics 47 (12) (2018) 2539–2560. doi:10.1002/eqe.3098.
URL http://doi.wiley.com/10.1002/eqe.3098

[34] V. Piccirillo, A. M. Tusset, J. M. Balthazar, OPTIMIZATION OF DYNAMIC VIBRATION ABSORBERS BASED ON EQUAL-PEAK THEORY, Lat. Am. J. Solids Struct. 16 (4) (2019) 1–22. doi:10.1590/1679-78255285.
URL http://www.scielo.br/scielo.php?script=sci_arttext&pid=S1679-78252019000400506&lng=en&tlng=en

[35] J. Štepánek, J. Máca, Design of Tuned Mass Dampers for Large Structures Using Modal Analysis, Acta Polytechnica CTU Proceedings 26 (2020) 100–106. doi:10.14311/APP.2020.26.0100.
URL https://ojs.cvut.cz/ojs/index.php/APP/article/view/6396

[36] A. Y. T. Leung, H. Zhang, C. C. Cheng, Y. Y. Lee, Particle swarm optimization of TMD by nonstationary base excitation during earthquake, Earthq. Eng. Struct. Dyn. 37 (9) (2008) 1223–1246. doi:10.1002/eqe.811.
URL http://doi.wiley.com/10.1002/eqe.811

[37] A. Leung, H. Zhang, Particle swarm optimization of tuned mass dampers, Eng. Struct. 31 (3) (2009) 715–728. doi:10.1016/j.engstruct.2008.11.017.
URL http://dx.doi.org/10.1016/j.engstruct.2008.11.017 https://linkinghub.elsevier.com/retrieve/pii/S01410296

[38] M. N. S. Hadi, Y. Arfiadi, Optimum Design of Absorber for MDOF Structures, J. Struct. Eng. 124 (11) (1998) 1272–1280. doi:10.1061/(ASCE)0733-9445(1998)124:11(1272).
URL http://ascelibrary.org/doi/10.1061/%28ASCE%290733-9445%281998%29124%3A11%281272%29

[39] Y. Arfiadi, M. N. S. Hadi, Optimum Placement and Properties of Tuned Mass Dampers Using Hybrid Genetic Algorithms, Int. J. Optim. Civ. Eng. 1 (2011) 167–187.
URL http://ijoce.iust.ac.ir/article-1-14-en.html

[40] M. Mohebbi, K. Shakeri, Y. Ghanbarpour, H. Majzoub, Designing optimal multiple tuned mass dampers using genetic algorithms (GAs) for mitigating the seismic response of structures, J. Vib. Control 19 (4) (2013) 605–625. doi:10.1177/1077546311434520.
URL http://journals.sagepub.com/doi/10.1177/1077546311434520

[41] G. Bekda, S. M. Nigdeli, Estimating optimum parameters of tuned mass dampers using harmony search, Eng. Struct. 33 (9) (2011) 2716–2723. doi:10.1016/j.engstruct.2011.05.024.
URL http://dx.doi.org/10.1016/j.engstruct.2011.05.024 https://linkinghub.elsevier.com/retrieve/pii/S01410296

[42] S. M. Nigdeli, G. Bekda, Optimum tuned mass damper design in frequency domain for structures, KSCE J. Civ. Eng. 21 (3) (2017) 912–922. doi:10.1007/s12205-016-0829-2.
URL http://link.springer.com/10.1007/s12205-016-0829-2

[43] H. Y. Zhang, L. J. Zhang, Tuned mass damper system of high-rise intake towers optimized by improved harmony search algorithm, Eng. Struct. 138 (2017) 270–282. doi:10.1016/j.engstruct.2017.02.011.
URL http://dx.doi.org/10.1016/j.engstruct.2017.02.011

[44] F. A. C. Viana, G. I. Kotinda, D. A. Rade, V. Steffen, Tuning dynamic vibration absorbers by using ant colony optimization, Computers & Structures 86 (13-14) (2008) 1539–1549. doi:10.1016/j.compstruc.2007.05.009.
URL https://linkinghub.elsevier.com/retrieve/pii/S0045794907001885

[45] A. Farshidianfar, S. Soheili, Ant colony optimization of tuned mass dampers for earthquake oscillations of high-rise structures including soilstructure interaction, Soil Dyn. Earthq. Eng. 51 (2013) 14–22. doi:10.1016/j.soildyn.2013.04.002.
URL http://dx.doi.org/10.1016/j.soildyn.2013.04.002 https://linkinghub.elsevier.com/retrieve/pii/S0267726113

[46] M.-y. Liu, W.-c. Liang, Y.-z. Lin, Simulated annealing optimization of tuned mass dampers for vibration control of seismic-excited buildings, Proc. 9th Int. Conf. Appl. Oper. Res. (ICAOR 2017) 9 (2017) 1–9.

[47] S. Salcedo-Sanz, C. Camacho-Gómez, A. Magdaleno, E. Pereira, A. Lorenzana, Structures vibration control via Tuned Mass Dampers using a co-evolution Coral Reefs Optimization algorithm, J. Sound Vib. 393 (2017) 62–75. doi:10.1016/j.jsv.2017.01.019.
URL http://dx.doi.org/10.1016/j.jsv.2017.01.019 https://linkinghub.elsevier.com/retrieve/pii/S0022460X173003

[48] F. Yang, R. Sedaghati, E. Esmailzadeh, Vibration suppression of curved beam-type structures using optimal multiple tuned mass dampers, J. Vib. Control 20 (6) (2014) 859–875. doi:10.1177/1077546312468461.
URL http://journals.sagepub.com/doi/10.1177/1077546312468461

[49] M. A. Woodbury, Inverting modified matrices, Memo. Rep. 42 (106) (1950) 336.

[50] T. Asami, O. Nishihara, A. M. Baz, Analytical Solutions to H[sub] and H[sub 2] Optimization of Dynamic Vibration Absorbers Attached to Damped Linear Systems, J. Vib. Acoust. 124 (2) (2002) 284. doi:10.1115/1.1456458.
URL http://vibrationacoustics.asmedigitalcollection.asme.org/article.aspx?articleid=1470416

[51] F. Petit, M. Loccufier, D. Aeyels, On the Attachment Location of Dynamic Vibration Absorbers, J. Vib. Acoust. 131 (3) (2009) 034501. doi:10.1115/1.3085888.
URL http://link.aip.org/link/?VAJ/131/034501/1 http://vibrationacoustics.asmedigitalcollection.asme.org/arti

[52] M. Géradin, D. J. Rixen, Mechanical vibrations: theory and application to structural dynamics, John Wiley & Sons, 2014.

[53] M. B. Ozer, T. J. Royston, Extending Den Hartog's Vibration Absorber Technique to Multi-Degree-of-Freedom Systems, J. Vib. Acoust. 127 (4) (2005) 341. doi:10.1115/1.1924642.
URL http://vibrationacoustics.asmedigitalcollection.asme.org/article.aspx?articleid=1470767

[54] B. Y. J. Sherman, W. J. Morrison, Adjustment of an Inverse Matrix Corresponding to a Change in One Element of a Given Matrix, Ann. Math. Stat. 21 (1) (1950) 124–127.
URL http://www.jstor.org/stable/2236561.

[55] P. D. Cha, N. C. Yoder, Applying Sherman-Morrison-Woodbury Formulas to Analyze the Free and Forced Responses of a Linear Structure Carrying Lumped Elements, J. Vib. Acoust. 129 (3) (2007) 307. doi:10.1115/1.2730537.
URL http://vibrationacoustics.asmedigitalcollection.asme.org/article.aspx?articleid=1470946

[56] J. Nocedal, S. J. Wright, Numerical optimization, Springer, 2006.

[57] N. Bruinsma, M. Steinbuch, A fast algorithm to compute the H-norm of a transfer function matrix, Systems & Control Letters 14 (4) (1990) 287–293. doi:10.1016/0167-6911(90)90049-Z.
URL https://linkinghub.elsevier.com/retrieve/pii/016769119090049Z